Bulletin of Mathematical Biology (2006) 68: 627–654
DOI 10.1007/s11538-005-9023-2

ORIGINAL ARTICLE

Convection Effects in the BIAcore Dextran Layer: Surface Reaction Model

David A. Edwards*

Department of Mathematical Sciences, University of Delaware, Newark, DE 19716-2553, USA

Received: 8 December 2004 / Accepted: 15 March 2005 / Published online: 7 April 2006

Abstract The BIAcore is a surface plasmon resonance (SPR) device used to measure rate constants, primarily for biochemical reactions. It consists of a flow channel containing one reactant adjoining a dextran gel containing the other. In order to explain anomalous measurements from the device, it has been proposed that some flow penetrates into the dextran layer, thus enhancing transport. A model is presented that accounts for such behavior, and typical velocity fields in the dextran are constructed. The system is analyzed in the limit of the surface reaction model, which corresponds to the limit of thin dextran layers. Asymptotic and singular perturbation techniques are used to analyze association and dissociation kinetics. Linear and nonlinear integral equations result from the analysis; explicit and asymptotic solutions are constructed for physically realizable cases. The results indicate that the effects of such penetration are bound to be small, regardless of the flow model used.

Keywords Asymptotic expansions · BIAcore · Biochemical reactions · Integrodifferential equations · Surface reaction

Nomenclature

Variables and parameters

Units are listed in terms of length (L), moles (N), or time (T). If the same letter appears both with and without tildes, the letter with a tilde has dimensions, while the letter without a tilde is dimensionless. The equation where a quantity first appears is listed, if appropriate.

*Corresponding address.
E-mail address: edwards@math.udel.edu (David A. Edwards).

a:	steric hindrance factor (23).
$\tilde{B}(\cdot, \tilde{t})$:	bound state concentration on surface at position $\cdot$ and time $\tilde{t}$; unit N/L^2 (23).
$\mathcal{C}$:	the Bromwich contour.
$\tilde{C}(\tilde{x}, \tilde{y}, \tilde{t})$:	unbound ligand concentration at position $(\tilde{x}, \tilde{y})$ and time $\tilde{t}$; unit N/L^3 (10).
$\tilde{D}$:	molecular diffusion coefficient; unit L^2/T (10).
Da:	Damköhler number, which measures the ratio of reaction and diffusion effects (15).
$f(\cdot)$:	arbitrary function.
H:	height of a portion of the channel; unit L (1a).
$h(x)$:	function used in effective rate constant solution (38).
$\mathcal{I}[\beta; x]$:	integration operator, defined in (51) as $\mathcal{I}[\beta; x] \equiv \int_0^x \beta(\xi)\,\mathrm{d}\xi$.
K:	dimensionless affinity constant for system (28a).
$\tilde{k}_{\mathrm{off}}$:	dissociation rate; unit T^{-1} (23).
$\tilde{k}_{\mathrm{on}}$:	binding rate; unit $L^3/(NT)$ (14a).
L:	length of the channel; unit L (1a).
m:	arbitrary constant.
$P(m/3, -\nu x)$:	normalized lower incomplete gamma function (53b).
Pe_{f}:	Peclét number for the system, which measures the ratio of convective to diffusive effects, defined as $V_{\mathrm{f}} H_{\mathrm{f}}^2/\tilde{D}_{\mathrm{f}} L$ (12).
Q:	flow rate through channel; unit L^3/T.
$\tilde{R}_{\mathrm{T}}$:	receptor sites; unit N/L^2 (15).
r:	dimensionless parameter (49a).
S:	slope of a line; unit T^{-1} (52).
s:	Laplace transform variable.
$\tilde{t}$:	dimensional time; unit T (10).
V:	characteristic velocity scale; unit L/T (3a).
$\tilde{v}(\tilde{y})$:	flow velocity; unit L/T (1a).
w:	width of channel; unit L.
$\tilde{x}$:	dimensional measure of length along the channel; unit L (10).
$\tilde{y}$:	dimensional measure of height from dextran–flow interface; unit L (1a).
$\mathcal{Z}$:	the integers.
α:	dimensionless constant, defined as $1 + K$ (34a).
$\beta(x)$:	term in expansion of $B(x, t)$ for small t (47).
Δp:	pressure differential; unit M/LT^2 (1a).
μ:	bulk viscosity; unit M/LT (1a).
ν:	dimensionless parameter (49b).
ξ:	dummy variable.
χ:	dimensionless constant, value $1 - \alpha B_{\mathrm{i}}$ (37).

Other notations

a: as a subscript, used to indicate an association experiment (49a).
d: as a subscript, used to indicate a dissociation experiment (58a).

f: as a subscript, used to indicate the flow region (1a).
g: as a subscript, used to indicate the dextran gel layer (1b).
i: as a subscript, used to indicate the initial state of a quantity (25).
max: as a subscript, used to indicate the right endpoint of the scanning range (31).
min: as a subscript, used to indicate the left endpoint of the scanning range (31).
$m \in \mathcal{Z}$: as a subscript, used to indicate an expansion in y_{f} (13a) or Da (33).
r: as a subscript, used to indicate a ratio of gel to flow (4).
s: as a subscript, used to indicate a steady state (41).
u: as a subscript on C, used to indicate a characteristic value (11).
∞: as a subscript on ν, used to indicate the value as $\tilde{k}_{\mathrm{on}} \to \infty$ (63).
$\bar{\ }$: used to denote the mean of the bound concentration (31).
$\hat{\ }$: used to indicate the Laplace transform of a quantity.

1. Introduction

To understand biological processes, scientists must have accurate measurements of the speed at which the underlying biochemical reactions occur. The relevant parameters in question are the *rate constants*, which relate directly to the rate of a reaction between well-mixed quantities, eliminating depletion and transport effects. Measurements of reaction rates can be most readily obtained from real-time measurements of the species evolution for a particular reaction. One popular device for obtaining such data is the BIAcore, which is a surface plasmon resonance (SPR) device.

The BIAcore has proven to be an extremely versatile instrument, aiding researchers in a variety of areas. Researchers are using the BIAcore to help design self-assembling DNA chips (Boireau et al., 2005). Varadarajan et al. (2005) used the BIAcore to characterize antibody–antigen reactions in the immune response, advancing their work towards an HIV vaccine. Because of the real-time nature of the device, Minunnia et al. (2005) are using the BIAcore to automate and greatly speed the process of identifying useful pharmaceutical compounds from plant samples. The speed with which the BIAcore can obtain measurements is exploited by Samsonova et al. (2004) to create a preliminary screen for shellfish exposure to environmental toxins.

The configuration of the BIAcore is described in great detail elsewhere (Karlsson et al., 1991; Liedberg et al., 1993; Szabo et al., 1995; Karlsson and Fält, 1997). For our purposes, the BIAcore device consists of a rectangular channel through which one of the reactants (the *ligand*) is convected in a standard two-dimensional Poiseuille flow from $\tilde{x} = 0$, the inlet position (see Fig. 1). The other reactant (the *receptor*) is bound to a sensor chip which is attached to the ceiling of the channel. Depending on its reactive characteristics, the receptor is either bound directly to the sensor's gold surface (in the case of a C1 chip) or embedded in a thin dextran gel that is linked to the gold surface (Hoffman et al., 2000). The latter case is the most prevalent, so we focus on it in this paper.

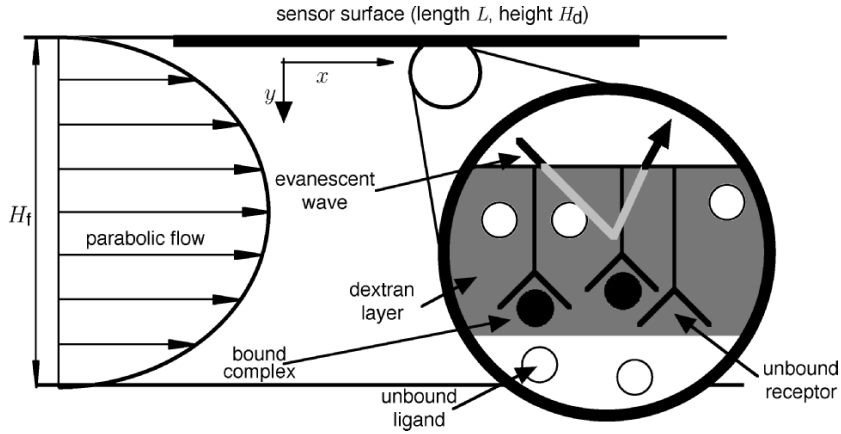

Fig. 1 Schematic of BIAcore device. Unbound ligand molecules are carried in parabolic flow from the left. The large circle illustrates a magnification of the area indicated by the smaller circle. In this region near the dextran layer, unbound ligand molecules migrate to empty receptor sites and bind.

Binding is measured by an evanescent wave that tracks mass changes in the sensor chip. This *sensogram* data is then transferred to a regression program that predicts the rate constants using an appropriate mathematical model. Mathematical models of the BIAcore have treated many facets of its dynamics and transport processes. The effects of convective transport and depletion along the channel are well-known (Davis et al., 1995; Myszka et al., 1998; Edwards, 1999; Edwards et al., 1999; Mason et al., 1999). The effects of diffusive processes in the dextran layer have been studied by Edwards (2001), Schuck (1996), Wofsy and Goldstein (2002), and Yarmush et al. (1996). Even the effects of the decay of the measuring wave in the BIAcore have been examined (Liedberg et al., 1993; Schuck, 1996; Edwards, 2004). However, discrepancies between measurements and simulations still occur (Karlsson and Fält, 1997; Witz, 1999; Qian, 2004).

In almost all of the BIAcore studies to date, the dextran gel is treated as a solid, and hence diffusion is the only transport process of interest. To explain some of the anomalous observations, Witz (1999) proposed that some of the buffer flow in the channel penetrated into the dextran gel. In this paper, we build on Witz's work by quantitatively describing the effect of flow penetration on the chemical reaction in the BIAcore.

To do so, we model the dextran gel as a viscous fluid. We derive the flow profiles in dextran and the channel, and then indicate how these profiles affect transport in the bulk flow. The relevant physical parameter for penetration is shown to be H_r, the ratio of the heights of the gel and bulk flow regions. When considering the binding, we focus on a surface reaction model, leaving the gel reaction model for later work (Edwards, submitted).

We show that the flow adds a local depletion term to the mass action law for the bound state. In the limit of small Damköhler number Da, we obtain explicit solutions for the bound state as well as expressions that can be easily fitted to sensogram data. When $Da = O(1)$, a nonlinear integral equation results, but the rate

constants can easily be estimated from a short-time solution for the bound-state concentration. We consider not only association, but also dissociation experiments.

As in Witz (1999), we show that flow penetration speeds transport. However, our results indicate that any enhancements to transport from flow penetration are very small. This conclusion arises from the small width of the gel layer, therefore using more sophisticated models for the dextran layer, such as a polymer brush model, will not change this fact. Thus, flow penetration may be safely ignored when using a surface reaction model to analyze BIAcore sensogram data.

2. Velocity profiles

We consider the BIAcore to consist of two regions, as shown in Fig. 1: the open channel (the region $0 \le \tilde{x} \le L$, $0 \le \tilde{y} \le H_f$, where the subscript "f" stands for "flow"), and the dextran gel layer (the region $0 \le \tilde{x} \le L$, $-H_g \le \tilde{y} \le 0$, where the subscript "g" stands for "gel"). In this section, we derive profiles for the flow velocity in each region.

The model for flow in the channel is the simple one-dimensional laminar flow, since the Reynolds number is small (see Appendix). The velocity $\tilde{v}$ is in the $\tilde{x}$-direction; thus we have

$$\mu_f \frac{d^2 \tilde{v}_f}{d\tilde{y}^2} = -\frac{\Delta p}{L}, \qquad 0 \le \tilde{y} \le H_f; \qquad \tilde{v}_f(H_f) = 0, \tag{1a}$$

where μ is the bulk viscosity and Δp is the (constant) pressure differential, which can be related to the known flow rate Q. The boundary condition is simple no-slip at the wall.

Next, we consider the thornier question of the flow field inside the dextran. Dextran is a gel, and hence any true description of the flow inside it would have to include porous media or other similar effects. For instance, Witz (1999) considers the gel to be a polymer brush. Initially we treat it merely as a very viscous fluid. Though this will necessarily misstate some quantitative features of the flow, we shall demonstrate that from the standpoint of analyzing sensogram data, such errors are negligible.

Note that we use the standard Eulerian coordinate frame when formulating our equations. If the dextran gel were a true fluid, this would cause the receptor sites to move with time, which would require a Lagrangian description of their dynamics. However, since the viscous fluid is only an (somewhat crude) approximation to the actual dextran gel, we may keep the receptor sites fixed in the Eulerian frame. One can envision this as the fluid flowing through a forest of receptors.

Thus, we model the flow in dextran as in (1a):

$$\mu_g \frac{d^2 \tilde{v}_g}{d\tilde{y}^2} = -\frac{\Delta p}{L}, \qquad -H_g \le \tilde{y} \le 0; \qquad \tilde{v}_g(-H_g) = 0. \tag{1b}$$

Note that the pressure differential in the two regions must be identical to maintain unidirectional flow. Finally, at the interface $\tilde{y} = 0$, we have continuity of velocity

and stress:

$$\tilde{v}_{\mathrm{f}}(0) = \tilde{v}_{\mathrm{g}}(0), \qquad \mu_{\mathrm{f}} \frac{\mathrm{d}\tilde{v}_{\mathrm{f}}}{\mathrm{d}\tilde{y}}(0) = \mu_{\mathrm{g}} \frac{\mathrm{d}\tilde{v}_{\mathrm{g}}}{\mathrm{d}\tilde{y}}(0). \tag{2}$$

To streamline the analysis, we introduce dimensionless variables. In the flow region, we use scalings chosen to simplify the algebra:

$$y_{\mathrm{f}} = \frac{\tilde{y}}{H_{\mathrm{f}}}, \qquad v_{\mathrm{f}}(y_{\mathrm{f}}) = \frac{\tilde{v}_{\mathrm{f}}(\tilde{y})}{V_{\mathrm{f}}}, \qquad V_{\mathrm{f}} = \frac{\Delta p H_{\mathrm{f}}^2}{2\mu_{\mathrm{f}} L}. \tag{3a}$$

There are several choices for the characteristic scale V_{g} for $\tilde{v}_{\mathrm{g}}$. We could keep the velocity interface condition balanced by choosing $V_{\mathrm{g}} = V_{\mathrm{f}}$. However, we know from the Appendix that $H_{\mathrm{g}} \ll H_{\mathrm{f}}$, so we expect the velocity in the dextran gel to be much lower than that in the bulk flow. This regime matches previous models that treat dextran as a solid with no velocity (Schuck, 1996; Yarmush et al., 1996; Edwards, 2001; Wofsy and Goldstein, 2002; Edwards, 2004). Alternatively, we could choose V_{g} to simplify (1b).

However, due to the small size of the channel and the larger bulk flow above, the main driving force for the velocity in dextran will not be the pressure differential modeled in (1b). Rather the shear stresses imposed by the bulk flow at $\tilde{y} = 0$, as modeled in (2), will dominate. Therefore, we introduce the following scalings, which keep the stress interface condition in (2) balanced:

$$y_{\mathrm{g}} = \frac{\tilde{y}}{H_{\mathrm{g}}}, \qquad v_{\mathrm{g}}(y_{\mathrm{g}}) = \frac{\tilde{v}_{\mathrm{g}}(\tilde{y})}{V_{\mathrm{g}}}, \qquad V_{\mathrm{g}} = \frac{H_{\mathrm{r}}}{\mu_{\mathrm{r}}} V_{\mathrm{f}}, \tag{3b}$$

$$H_{\mathrm{r}} = \frac{H_{\mathrm{g}}}{H_{\mathrm{f}}}, \qquad \mu_{\mathrm{r}} = \frac{\mu_{\mathrm{g}}}{\mu_{\mathrm{f}}}. \tag{4}$$

Here the subscript "r" refers to "ratio," and we will use it in the same way (gel to flow) throughout.

Since solid dextran corresponds to $\mu_{\mathrm{r}} = \infty$, we might consider μ_{r} as a large parameter to use in a perturbation approach. This is not the best choice, for we can solve our problem for *any* μ_{r} if we use a different perturbation parameter, as described later.

Substituting (3) and (4) into (1), we obtain

$$\frac{\mathrm{d}^2 v_{\mathrm{f}}}{\mathrm{d}y_{\mathrm{f}}^2} = -2, \quad 0 \le y_{\mathrm{f}} \le 1; \quad v_{\mathrm{f}}(1) = 0, \tag{5a}$$

$$\frac{\mathrm{d}^2 v_{\mathrm{g}}}{\mathrm{d}y_{\mathrm{g}}^2} = -2H_{\mathrm{r}}, \quad -1 \le y_{\mathrm{g}} \le 0; \quad v_{\mathrm{g}}(-1) = 0, \tag{5b}$$

$$v_{\mathrm{f}}(0) = \frac{H_{\mathrm{r}}}{\mu_{\mathrm{r}}} v_{\mathrm{g}}(0), \qquad \frac{\mathrm{d}v_{\mathrm{f}}}{\mathrm{d}y_{\mathrm{f}}}(0) = \frac{\mathrm{d}v_{\mathrm{g}}}{\mathrm{d}y_{\mathrm{g}}}(0). \tag{6}$$

As desired, the stress interface equation remains balanced in the dimensionless context. Solving (5) and (6), we have the following results:

$$v_{\mathrm{f}}(y_{\mathrm{f}}) = 1 - y_{\mathrm{f}}^2 + \frac{(y_{\mathrm{f}} - 1)(\mu_{\mathrm{r}} - H_{\mathrm{r}}^2)}{H_{\mathrm{r}} + \mu_{\mathrm{r}}}, \tag{7a}$$

$$v_{\mathrm{g}}(y_{\mathrm{g}}) = H_{\mathrm{r}}(1 - y_{\mathrm{g}}^2) + \frac{(y_{\mathrm{g}} + 1)(\mu_{\mathrm{r}} - H_{\mathrm{r}}^2)}{H_{\mathrm{r}} + \mu_{\mathrm{r}}}. \tag{7b}$$

In order to calculate V_{f} for any experiment, we relate the velocity profiles to the known flow rate Q. If the channel has width w, then we have

$$\frac{Q}{w} = \int_{-H_{\mathrm{g}}}^{0} \tilde{v}_{\mathrm{g}}(\tilde{y})\,\mathrm{d}\tilde{y} + \int_{0}^{H_{\mathrm{f}}} \tilde{v}_{\mathrm{f}}(\tilde{y})\,\mathrm{d}\tilde{y}.$$

Substituting our velocity results from (7) into the above, we obtain the following result for the dimensionless flux $Q/wV_{\mathrm{f}}H_{\mathrm{f}}$:

$$\frac{Q}{wV_{\mathrm{f}}H_{\mathrm{f}}} = \frac{2}{3} - \frac{1 - H_{\mathrm{r}}^2/\mu_{\mathrm{r}}}{2(1 + H_{\mathrm{r}}/\mu_{\mathrm{r}})} + \frac{H_{\mathrm{r}}^2}{\mu_{\mathrm{r}}}\left[\frac{2H_{\mathrm{r}}}{3} + \frac{1 - H_{\mathrm{r}}^2/\mu_{\mathrm{r}}}{2(1 + H_{\mathrm{r}}/\mu_{\mathrm{r}})}\right]. \tag{8}$$

From the Appendix, we have that $H_{\mathrm{r}} = 2 \times 10^{-3}$ as an upper bound, so the dextran layer is only 1/500 as thick as the bulk. Thus, we choose H_{r} as the small perturbation parameter characterizing this aspect of the problem. (Other dimensionless parameters will characterize other dynamic processes, as shown later.) Expanding (8) for small H_{r}, we have

$$\frac{Q}{wV_{\mathrm{f}}H_{\mathrm{f}}} = \frac{1}{6} + O\left(\frac{H_{\mathrm{r}}}{\mu_{\mathrm{r}}}\right). \tag{9}$$

The 1/6 value in (9) is exactly the value of the dimensionless flux when the reacting layer is treated as a surface. Note that the behavior of the flow for large μ_{r} follows naturally from this expansion, as μ_{r} is always coupled with H_{r} in (8). Since we expect the effective viscosity of the dextran to be high, μ_{r} is quite large, and the error we make in using (9) is therefore quite small.

In the limit of small H_{r}, (7b) becomes a nearly linear profile, corresponding to shear-driven flow. A more complicated polymer brush model for the dextran layer leads to exponential and Bessel function profiles for the velocity field (Witz, 1999). Nevertheless, that author reduces these complicated functions to linear profiles in the region of interest. Thus, the two approaches are equivalent with proper choices of μ_{r}.

3. Transport in the flow

In the flow, the ligand (concentration $\tilde{C}$) travels both by convection and diffusion:

$$\frac{\partial \tilde{C}_{\mathrm{f}}}{\partial \tilde{t}} = \tilde{D}_{\mathrm{f}}\left(\frac{\partial^2 \tilde{C}_{\mathrm{f}}}{\partial \tilde{x}^2} + \frac{\partial^2 \tilde{C}_{\mathrm{f}}}{\partial \tilde{y}^2}\right) - \tilde{v}_{\mathrm{f}}(\tilde{y})\frac{\partial \tilde{C}_{\mathrm{f}}}{\partial \tilde{x}}, \tag{10}$$

where $\tilde{D}_f$ is the molecular diffusion coefficient of the ligand in the flow. At the upstream end ($\tilde{x} = 0$), we have a prescribed concentration C_u:

$$\tilde{C}_f(0, \tilde{y}, \tilde{t}) = C_u. \tag{11}$$

For the BIAcore system, the Peclét number (Pe_f) in the flow, given by

$$Pe_f = \frac{H_f^2/\tilde{D}_f}{L/V_f} = \frac{\text{Characteristic diffusion time in flow}}{\text{Characteristic convection time in flow}}, \tag{12}$$

is large (for a typical value, see Table 2 later). Hence, one need consider only the thin Lévêque boundary layer near $\tilde{y} = 0$ (Edwards, 1999). Thus, we expand (7a) for small y_f to obtain

$$v_f(y_f) = v_f(0) + v_1 y_f, \qquad v_f(0) = \frac{H_r(H_r + 1)}{H_r + \mu_r}, \tag{13a}$$

$$v_1 \equiv v_f'(0) = \frac{\mu_r - H_r^2}{H_r + \mu_r}. \tag{13b}$$

In the case that $\mu_r = \infty$, $v_f(y_f) \sim y_f$, which is the standard normalized velocity profile for a no-slip condition (Edwards, 1999).

Our results should reduce to solid dextran when $\mu_r \to \infty$, so we use the scalings from Edwards (2001), which treats that case:

$$x = \frac{\tilde{x}}{L}, \qquad y = Pe_f^{1/3} y_f = \frac{Pe_f^{1/3}\tilde{y}}{H_f}, \qquad t = \tilde{k}_{on} C_u \tilde{t}, \tag{14a}$$

where $\tilde{k}_{on}$ is the association rate constant for the binding reaction. (Hence the time scale of interest is the one on which the reaction occurs.)

Motivated by Edwards (2004), we scale the ligand concentration in the following way:

$$\tilde{C}_f(\tilde{x}, \tilde{y}, \tilde{t}) = C_u[1 - Da\, C_f(x, y, t)]. \tag{14b}$$

Here C_u is the inlet value of the ligand concentration. Thus the relevant quantity for the ligand concentration is the new dependent variable C_f (Edwards, 1999). Once multiplied by the Damköhler number (Da), C_f represents the percentage change in ligand concentration from the upstream value. It will be shown later that the driving force for this change is the depletion of ligand due to binding at the surface.

The Damköhler number is defined as

$$Da = \frac{\tilde{k}_{on}\tilde{R}_T}{\tilde{D}_f/(H_f Pe_f^{-1/3})} = \frac{\text{Reaction "velocity"}}{\text{Diffusion "velocity" in boundary layer}}, \tag{15}$$

where $\tilde{R}_T$ is the density of receptor sites in the device. It is an area density, which means for a problem with a dextran gel layer, it is simply the volume density

averaged over the $\tilde{y}$-direction. Though the receptor density may initially be nonuniform (O'Shannessy et al., 1992; Joss et al., 1998) for now we take it to be uniform, since the error introduced from such an assumption is small (Edwards and Swaminathan, 2005).

As discussed earlier, Da measures the effect of transport on the chemical reaction. In particular, from (14b) we see that it characterizes the size of ligand depletion induced by the reaction. Since $Pe_\mathrm{f} \propto V_\mathrm{f}$, $Da = 0$ corresponds to the case of infinitely fast flow where no depletion occurs. The reasoning behind the choice for the Da scaling in (14b) will become clear shortly. Because the ligand concentration can never exceed the input value, $C_\mathrm{f} \geq 0$.

Substituting (14) and (13a) into (10), we obtain

$$k_\mathrm{on} Pe_\mathrm{f}^{1/3} \frac{\partial C_\mathrm{f}}{\partial t} = \frac{\partial^2 C_\mathrm{f}}{\partial y^2} - \left[Pe_\mathrm{f}^{1/3} v_\mathrm{f}(0) + v_1 y + O\left(Pe_\mathrm{f}^{-1/3}\right) \right] \frac{\partial C_\mathrm{f}}{\partial x}, \tag{16a}$$

$$k_\mathrm{on} = \frac{\tilde{k}_\mathrm{on} C_\mathrm{u} L}{V_\mathrm{f}}, \tag{16b}$$

where we have used the fact that $Pe_\mathrm{f} \gg 1$ in eliminating the x-diffusion term. As noted in Edwards (1999), $k_\mathrm{on} Pe_\mathrm{f}^{1/3} \ll 1$, and hence we are in the steady state of the flow transport equation.

From (16a) we see that if $v_\mathrm{f}(0)$ is larger than $O(Pe_\mathrm{f}^{-1/3})$, that term dominates and we must rescale y. For instance, if $v_\mathrm{f}(0) = O(1)$, we must choose a scaling of $Pe_\mathrm{f}^{1/2}$ to balance the x- and y-diffusion terms. However, such a choice is unsatisfactory for several reasons:

1. We want to replicate our previous results in the case where $\mu_\mathrm{r} \to \infty$; therefore, we want our scalings to remain the same, not jump from $Pe_\mathrm{f}^{1/2}$ to $Pe_\mathrm{f}^{1/3}$.
2. As discussed earlier, $v_\mathrm{f}(0) \neq O(1)$; it is small. Nevertheless, we do not take $v_\mathrm{f}(0) = O(Pe_\mathrm{f}^{-1/3})$ and ignore it, since we want the effect of v_0 to appear at leading order.

Therefore, we choose the dominant balance of

$$v_\mathrm{f}(0) = v_0 Pe_\mathrm{f}^{-1/3}, \qquad v_0 = \frac{H_\mathrm{r} Pe_\mathrm{f}^{1/3}(H_\mathrm{r}+1)}{H_\mathrm{r} + \mu_\mathrm{r}}. \tag{17}$$

We may motivate this choice physically by noting that in order for the relative size of the transport effects to be comparable, the length scale in the boundary and dextran layers should be comparable. For instance, the diffusion time should be comparable, given that $\tilde{D}_\mathrm{g}$ and $\tilde{D}_\mathrm{f}$ have been determined to be of the same order (Phillies, 1985; Karlsson et al., 1994; Sikavitsas et al., 2002). Such a restriction yields

$$H_\mathrm{g} = O\left(H_\mathrm{f} Pe_\mathrm{f}^{-1/3}\right) \Longrightarrow H_\mathrm{r} = O\left(Pe_\mathrm{f}^{-1/3}\right). \tag{18}$$

Substituting (18) into (13a) yields the scaling in (17) as long as we treat μ_r as $O(1)$. This motivates the choice of H_r as a small parameter, since $Pe_\mathrm{f} \gg 1$.

Unfortunately,(18) is rather a weak bound. From the Appendix we have that $H_r = 2 \times 10^{-3}$ as an upper bound, while $Pe_f^{-1/3} = 1.39 \times 10^{-1}$. Thus, the dextran layer is quite a bit thinner than the unstirred layer, and so velocities there will be comparatively small.

With these assumptions, the leading order of (16a) becomes

$$\frac{\partial^2 C_f}{\partial y^2} = (v_0 + v_1 y)\frac{\partial C_f}{\partial x}. \tag{19}$$

If we recall that the case of solid dextran corresponds to $v_0 = 0$, we reduce to the previous case (Edwards, 2001). Lastly, we posit boundary conditions for (19). Substituting (14) into (11) yields the proper inlet condition:

$$C_f(0, y, t) = 0. \tag{20a}$$

The solution as we exit the boundary layer must match the concentration in the bulk, which does not deviate from the inlet concentration value. In dimensionless form, this condition becomes

$$C_f(x, \infty, t) = 0. \tag{20b}$$

To solve for C_f, we introduce the concept of the Laplace transform in the x-direction:

$$\hat{f}(s) = \int_0^\infty f(x)\mathrm{e}^{-sx}\,\mathrm{d}x, \qquad f(x) = \frac{1}{2\pi i}\int_{\mathcal{C}} \hat{f}(s)\mathrm{e}^{sx}\,\mathrm{d}s,$$

where $\mathcal{C}$ is the Bromwich contour. Taking the Laplace transform of (19) subject to (20a), we obtain

$$\frac{\partial^2 \hat{C}_f}{\partial y^2} = s(v_0 + v_1 y)\hat{C}_f,$$

the solution of which, subject to the Laplace transform of (20b), is

$$\hat{C}_f(s, y, t) = f(t)\,\mathrm{Ai}\left(\frac{s^{1/3}(v_0 + v_1 y)}{v_1^{2/3}}\right), \tag{21}$$

where $f(t)$ is an undetermined function. In general, $f(t)$ would be determined once we couple the flow to the reaction process.

Such coupling will take place at the flow–dextran interface $y = 0$, and therefore, we are interested in the value of $\hat{C}_f$ only at that point. In particular, we may eliminate the unknown function $f(t)$ from our analysis by noting that

$$\hat{C}_f(s, 0, t) = \frac{\mathrm{Ai}\left(s^{1/3}v_0/v_1^{2/3}\right)}{(sv_1)^{1/3}\,\mathrm{Ai}'\left(s^{1/3}v_0/v_1^{2/3}\right)}\frac{\partial \hat{C}_f}{\partial y}(s, 0, t). \tag{22}$$

4. Surface reaction model

Now we examine the reaction process. As a first attempt, we model the reaction by treating the receptor layer as a surface. It may seem inconsistent to consider the layer to find the velocity in Section 2 and then ignore it here. However, we note the following:

1. We could have just as easily derived (19) by modeling the flow in the dextran layer as a slip condition on the main flow, and calculating the slip size using dominant-balance arguments.
2. We know from Edwards (2001) that when including the receptor layer, transport effects in the x- and y-directions decouple, with the former arising directly from a surface reaction model. Thus, the results derived here will be useful when including the receptor layer in the reaction process (Edwards, submitted).

Treating the layer as a surface requires the introduction of the *area* concentration $\tilde{B}$ of bound receptors, which evolves according to a standard bimolecular mass action law:

$$\frac{\partial \tilde{B}}{\partial \tilde{t}} = \tilde{k}_{\text{on}}[(\tilde{R}_{\text{T}} - a\tilde{B})\tilde{C}_{\text{f}}(\tilde{x}, 0, \tilde{t})] - \tilde{k}_{\text{off}}\tilde{B}, \tag{23}$$

where $\tilde{k}_{\text{on}}$ and $\tilde{k}_{\text{off}}$ are the association and dissociation rate constants, respectively. The $(\tilde{R}_{\text{T}} - a\tilde{B})$ term models the number of receptors available for binding. Note that for each bound molecule, a receptors are unavailable for binding. a is a *steric hindrance factor*, which measures the ability of a ligand molecule to occlude neighboring receptors (Zheng and Rundell, 2003). By taking $a = 1$, we ignore this effect, since the only receptor unavailable for binding is the one actually bound.

To couple the flow and the reaction, we note that all diffusive flux into the reacting surface must be used up in binding:

$$\tilde{D}_{\text{f}}\frac{\partial \tilde{C}_{\text{f}}}{\partial \tilde{y}}(\tilde{x}, 0, \tilde{t}) = \frac{\partial \tilde{B}}{\partial \tilde{t}}. \tag{24}$$

Lastly, we impose an initial condition on $\tilde{B}$. Though the theory can handle general initial conditions, in practice the initial condition is always spatially uniform. For an association experiment, initially there is no bound state. For a dissociation experiment, we start with the steady state of (23), which will be shown to be a constant. Thus, we have

$$\tilde{B}(\tilde{x}, 0) = \tilde{B}_{\text{i}}, \tag{25}$$

where $\tilde{B}_{\text{i}}$ is a constant.

To scale $\tilde{B}$, we choose the receptor density:

$$B(x, t) = \frac{\tilde{B}(\tilde{x}, \tilde{t})}{\tilde{R}_{\text{T}}}, \qquad B_{\text{i}} = \frac{\tilde{B}_{\text{i}}}{\tilde{R}_{\text{T}}}. \tag{26}$$

Substituting (14) and (26) into (23)–(25) (with $a = 1$), we obtain

$$\frac{\partial C_\mathrm{f}}{\partial y}(x,0,t) = -\frac{\partial B}{\partial t}, \tag{27}$$

$$\frac{\partial B}{\partial t} = (1-B)\left[1 - Da\, C_\mathrm{f}(x,0,t)\right] - KB, \quad K = \frac{\tilde{k}_\mathrm{off}}{\tilde{k}_\mathrm{on} C_\mathrm{u}}, \tag{28a}$$

$$B(x,0) = B_\mathrm{i}. \tag{28b}$$

Here K is the dimensionless affinity constant.

Taking the Laplace transform of (27) and using (22), we have

$$\frac{\partial \hat{C}_\mathrm{f}}{\partial y}(s,0,t) = -\frac{\mathrm{d}\hat{B}}{\mathrm{d}t} \Longrightarrow \hat{C}_\mathrm{f}(s,0,t) = -\frac{\mathrm{Ai}\left(s^{1/3}v_0/v_1^{2/3}\right)}{(sv_1)^{1/3}\,\mathrm{Ai}'\left(s^{1/3}v_0/v_1^{2/3}\right)}\frac{\mathrm{d}\hat{B}}{\mathrm{d}t}. \tag{29}$$

(Note that we may use the total derivative for $\mathrm{d}\hat{B}/\mathrm{d}t$, since it depends only parametrically on s.) Since we cannot invert (29) in closed form, we use the fact that we consider dextran to be a very thick fluid, so $v_0 \to 0$. Formally, there are two ways to justify this from (17). The first, physically intuitive reasoning is to say that $\mu_\mathrm{r} \to \infty$. The second, more consistent from a mathematical point of view, is to take $H_\mathrm{r} \to 0$.

Then expanding (29) to leading two orders, we obtain the following:

$$\hat{C}_\mathrm{f}(s,0,t) \sim -\frac{1}{(sv_1)^{1/3}}\frac{\mathrm{d}\hat{B}}{\mathrm{d}t}\left\{\frac{\mathrm{Ai}(0)}{\mathrm{Ai}'(0)} + \frac{s^{1/3}v_0}{v_1^{2/3}} \times \left[\frac{\mathrm{Ai}'(0)}{\mathrm{Ai}'(0)} - \frac{\mathrm{Ai}(0)\,\mathrm{Ai}''(0)}{\mathrm{Ai}'(0)^2}\right] + O(v_0^2)\right\}, \tag{30a}$$

$$C_\mathrm{f}(x,0,t) = \frac{1}{(3v_1)^{1/3}\Gamma(2/3)}\int_0^x \frac{\partial B}{\partial t}(x-\xi,t)\frac{\mathrm{d}\xi}{\xi^{2/3}} - \frac{v_0}{v_1}\frac{\partial B}{\partial t} + O(v_0^2). \tag{30b}$$

The integral term in (30b) has an elegant physical interpretation. It merely states that the deficit in the ligand concentration at position x is the accumulation of the reaction that has occurred upstream. The effect of the slip velocity is to introduce the *local* reaction into the computation of the concentration deficit through the second term in (30b). With $v_0 = 0$ (which corresponds to $v_1 = 1$), (30b) reduces to the previous result in the surface reaction case in Edwards and Jackson (2002).

In our expansion in (30a), we tacitly assumed that $s^{1/3}v_0 \ll 1$. But Laplace transform theory states that small x corresponds to large s, therefore (30b) does not hold in the limit of small x. Fortunately, the BIAcore returns measurements not of B, but of the average of B over some scanning range $x_\mathrm{min} \le x \le x_\mathrm{max}$:

$$\bar{B}(t) = \frac{1}{x_\mathrm{max} - x_\mathrm{min}}\int_{x_\mathrm{min}}^{x_\mathrm{max}} B(x,t)\,\mathrm{d}x, \tag{31}$$

where $x_{\min}$ is bounded away from zero. Since $x = 0$ is out of the range of interest for the averaging in our device, we may confidently use (30b) to analyze sensogram data.

Substituting (30b) into (28a) and rearranging, we have

$$\frac{\partial B}{\partial t} + KB = (1 - B)\left\{1 - Da\left[\frac{1}{(3v_1)^{1/3}\Gamma(2/3)}\int_0^x \frac{\partial B}{\partial t}(x - \xi, t) \times \frac{\mathrm{d}\xi}{\xi^{2/3}} - \frac{v_0}{v_1}\frac{\partial B}{\partial t}\right]\right\}. \tag{32}$$

Equation (32) is a nonlinear integrodifferential equation, and an exact solution would have to be obtained numerically. However, asymptotic results can be derived in physically relevant regimes.

5. Small *Da* results

When designing experiments, scientists strive to keep *Da* as small as possible (Ward and Winzor, 2000). From (28a) one can see that the case of $Da = 0$ corresponds to the well-mixed case where there is no depletion. In order to keep $Da \ll 1$, the following bound on the velocity (and hence the flow rate) must be observed (Edwards, 2001):

$$V_{\mathrm{f}} \gg \frac{\tilde{k}_{\mathrm{on}}^3 \tilde{R}_{\mathrm{T}}^3 H_{\mathrm{f}} L}{\tilde{D}_{\mathrm{f}}^2}.$$

Clearly the faster the reaction, the higher the flow rate must be to minimize downstream depletion effects. Though the bound for V_{f} involves the unknown rate constant $\tilde{k}_{\mathrm{on}}$, one can obtain an order-of-magnitude estimate through even unadjusted calculations.

Therefore, we now specialize to the case of small *Da* by introducing the following expansion:

$$B(x, t) = B_0(x, t) + Da\, B_1(x, t) + O(Da). \tag{33}$$

5.1. *Association experiment*

We begin by considering an association experiment as described in Section 3.

Substituting (33) into (28a), we have, to leading two orders:

$$\frac{\partial B_0}{\partial t} = 1 - \alpha B_0, \quad \alpha = K + 1, \tag{34a}$$

$$B_0(x, 0) = B_{\mathrm{i}}, \tag{34b}$$

$$\frac{\partial B_1}{\partial t} + \alpha B_1 = -(1 - B_0)C_{\mathrm{f}}(x, 0, t), \quad B_1(x, 0) = 0. \tag{35}$$

Solving (34a) subject to (34b), we obtain

$$B_0(x,t) = \frac{1-\mathrm{e}^{-\alpha t}}{\alpha} + B_\mathrm{i}\mathrm{e}^{-\alpha t} = \bar{B}_0(t). \tag{36}$$

In order to calculate C_f, we first calculate the integrand in (30b):

$$\frac{\mathrm{d}B_0}{\mathrm{d}t} = \mathrm{e}^{-\alpha t}\chi, \qquad \chi = 1-\alpha B_\mathrm{i}. \tag{37}$$

The fact that B_0 is independent of x is critical; hence we emphasize this fact by using the total derivative in (37). Since (37) is independent of x, we may pull it out of the integral in (30b) to obtain

$$C_\mathrm{f}(x,0,t) = \frac{\mathrm{d}B_0}{\mathrm{d}t}h(x), \qquad h(x) = \frac{3^{2/3}x^{1/3}}{v_1^{1/3}\Gamma(2/3)} - \frac{v_0}{v_1}. \tag{38}$$

Substituting (36)–(38) into (35) and solving, we have the following:

$$B_1(x,t) = \left[\frac{(\mathrm{e}^{-\alpha t}-1)\chi}{\alpha} - Kt\right]\frac{\chi\mathrm{e}^{-\alpha t}h(x)}{\alpha}.$$

Then averaging, we have

$$\bar{B}_1(t) = \left[\frac{(\mathrm{e}^{-\alpha t}-1)\chi}{\alpha} - Kt\right]\frac{\chi\mathrm{e}^{-\alpha t}\bar{h}}{\alpha}, \tag{39a}$$

$$\bar{h} = \frac{3^{5/3}\left(x_\mathrm{max}^{4/3} - x_\mathrm{min}^{4/3}\right)}{4v_1^{1/3}\Gamma(2/3)(x_\mathrm{max}-x_\mathrm{min})} - \frac{v_0}{v_1}, \tag{39b}$$

where we have used (38).

Careful students of perturbation theory will note the term in (39a) proportional to $t\mathrm{e}^{-\alpha t}$, similar to a secularity in a two-timing exercise. This is not a problem from a practical perspective, since as $t\to\infty$, $B_0 = O(1)$ and $Da\, B_1 \ll B_0$. However, it can be shown (Edwards, 1999; Edwards et al., 1999) that a multiple-scale expansion is formally required. Though we could construct such an expansion for this case, it will not be illuminating.

To plot our solutions, we use the parameters listed in Tables 1 and 2, which are from Edwards (1999). The choice of H_r is discussed in the Appendix of this work.

Since the new facet of this work is the introduction of a viscous-fluid model for dextran, the salient feature is the effect of μ_r on the perturbation solution given

Table 1 Parameter values for Figs. 2 and 3.

Parameter	Value
B_i	0
χ	1

Table 2 Parameter values for Figs. 2–5.

Parameter	Value
C_T (mol cm^{-3})	10^{-11}
Da	10^{-1}
H_r	2×10^{-3}
K	1
$\tilde{k}_{on}$(cm^{3}mol^{-1}s^{-1})	10^8
Pe_f	3.72×10^2
t	$10^{-3}\,\tilde{t}$/s
x_{max}	7.92×10^{-1}
x_{min}	2.08×10^{-1}
α	2

by (36) and (39a). Figure 2 illustrates this effect by showing the *difference* between the perturbation solution for the solid dextran ($\mu_r = \infty$) case and the case of finite μ_r. The graph uses the *dimensional* time $\tilde{t}$ (in seconds) for better comparison with the sensogram data. Note that in every case the difference is quite small due to the low value of H_r. In particular, even the error for $\mu_r = 1$ (corresponding to the absence of a dextran layer) is only $O(H_r)$. In addition, the difference is positive; that is, allowing the flow to penetrate into the dextran layer enhances the association process, as suggested by Witz (1999).

These results may be stated more simply in the context of an *effective rate constant* equation (ERC), as outlined in Edwards (2001), Edwards et al. (1999), and Mason et al. (1999). Substituting (38) into (28a), we obtain

$$\frac{\partial B}{\partial t} = (1 - B)\left[1 - Da\,\frac{\mathrm{d}B_0}{\mathrm{d}t}h(x)\right] - KB + O(Da^2),$$

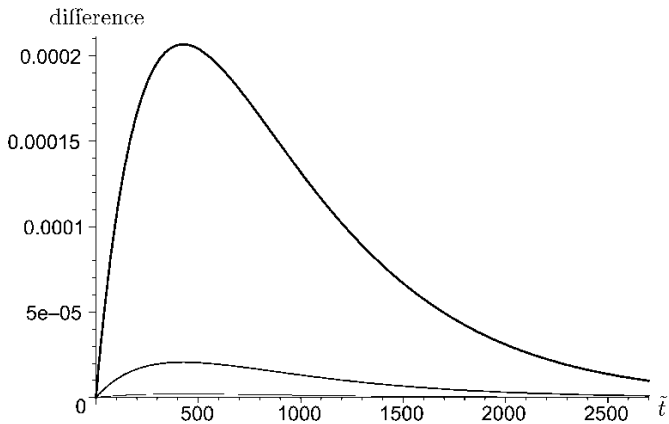

Fig. 2 Difference between perturbation solution with $\mu_r = \infty$ (solid dextran) and μ_r finite for (in decreasing order of thickness) $\mu_r = 1, 10, 100$. Association experiment.

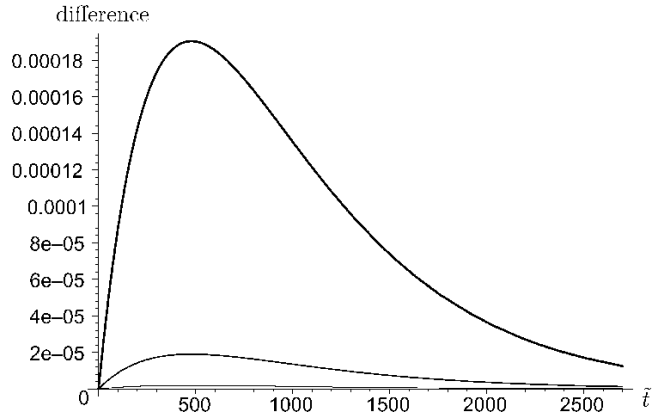

Fig. 3 Difference between ERC solution of (40) with $\mu_r = \infty$ (solid dextran) and μ_r finite for (in decreasing order of thickness) $\mu_r = 1, 10, 100$. Association experiment.

which we may rearrange and average to obtain

$$\frac{d\bar{B}}{dt} = \frac{1 - \alpha\bar{B}}{1 + Da(1 - \bar{B})\bar{h}} + O(Da^2). \tag{40}$$

Equation (40) is an ODE for $\bar{B}$, the actual sensogram data returned by the BIAcore. As such, it requires no post-processing averaging step. Equation (40) is in the form obtained previously (Edwards et al., 1999), albeit with a different value of $\bar{h}$. This is consistent with Edwards (2000), where it is shown that the ERC approximation is robust to various geometries and flows as long as B_0 is spatially uniform.

Since the form of (40) is more convenient for data analysis, we also present results showing the effect of the viscous-dextran assumption on the ERC solution. Again, we focus on the difference between the ERC solution with μ_r infinite (the solid dextran case) and the case with μ_r finite. The results are presented in Fig. 3. As before, flow penetration enhances the association process, but only slightly.

5.2. Dissociation experiment

We conclude this section with a brief discussion of dissociation experiments. In a typical BIAcore experimental run, an association experiment is run to completion. Then the ligand is removed from the buffer solution, and pure solution (inlet concentration $\tilde{C}_f = 0$) is injected into the device. This then provides additional data for rate constant estimation.

From (29) we see that as $t \to \infty$, $C_f(x, 0, t) \to 0$, so the steady state of (28a) is

$$B_s = \alpha^{-1}, \tag{41}$$

where the subscript "s" refers to the steady state. Equation (41) provides the initial condition for the dissociation problem, and hence we are justified in (25) in always taking the initial condition for B to be spatially uniform.

The equation analogous to (28a) is

$$\frac{\partial B}{\partial t} = (1 - B)[-Da\, C_{\mathrm{f}}(x, 0, t)] - KB. \tag{42}$$

Since no ligand is being injected into the device, the 1 inside the bracketed term in (28a) no longer appears. For consistency of our algebraic expressions, we wish to retain the sign of the remaining term. Physically, this term represents the concentration of ligand molecules introduced into the flow by dissociation from the bound state. Since this term must be positive, $C_{\mathrm{f}} \leq 0$ in the dissociation case, while it was non-negative in the association case.

Substituting (33) into (42) and (41), we have, to leading two orders,

$$\frac{\partial B_0}{\partial t} = -KB_0, \quad B_0(x, 0) = \alpha^{-1}, \tag{43a}$$

$$\frac{\partial B_1}{\partial t} + KB_1 = -(1 - B_0)C_{\mathrm{f}}(x, 0, t), \quad B_1(x, 0) = 0. \tag{43b}$$

Solving (43a), we obtain

$$B_0(x, t) = \bar{B}_0(t) = \frac{\mathrm{e}^{-Kt}}{\alpha}, \tag{44a}$$

$$\frac{\mathrm{d}B_0}{\mathrm{d}t} = -\frac{K\mathrm{e}^{-Kt}}{\alpha}. \tag{44b}$$

The form of Eq. (38) does not change; the only difference is that (44b) replaces (37). Since $\mathrm{d}B_0/\mathrm{d}t < 0$, $C_{\mathrm{f}} < 0$, as required. Substituting (38) and (44a) into (43b) and solving, we have the following:

$$B_1(x, t) = \frac{K}{\alpha}\left(t + \frac{\mathrm{e}^{-Kt} - 1}{K\alpha}\right) h(x)\mathrm{e}^{-Kt},$$

which we may average to obtain

$$\bar{B}_1(t) = \frac{K}{\alpha}\left(t + \frac{\mathrm{e}^{-Kt} - 1}{K\alpha}\right) \bar{h}\mathrm{e}^{-Kt}, \tag{45}$$

where $\bar{h}$ is given in (39b). The same secularity problem arises, but here it is more obvious since $Da\,\bar{B}_1 \gg \bar{B}_0$ as $t \to \infty$. Again, we restrict ourselves to the case where $Da\, t = O(1)$, since constructing the multiple-scale expansion is not illuminating.

Figure 4 is analogous to Fig. 2, as it shows the effect of varying μ_{r} on the perturbation solution for the dissociation experiment. Again, the difference between the solution with μ_{r} infinite and μ_{r} finite is graphed. In contrast to the association case, the difference is negative. By causing the function $\bar{B}_1$ to decay faster, penetration of the flow into the dextran layer enhances the dissociation process.

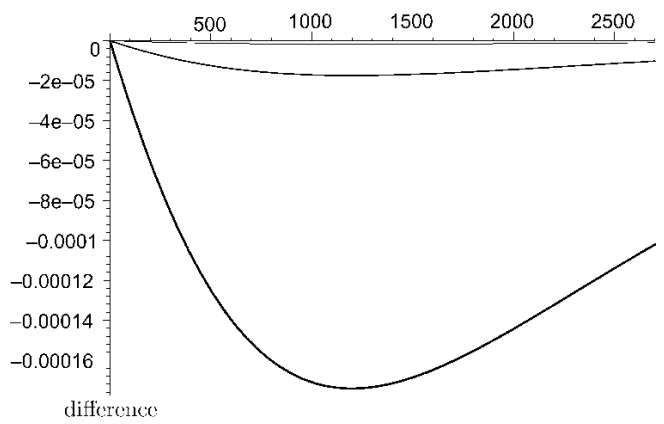

Fig. 4 Difference between perturbation solution with $\mu_r = \infty$ (solid dextran) and μ_r finite for (in decreasing order of thickness) $\mu_r = 1, 10, 100$. Dissociation experiment.

Since the value 1 is absent from the concentration term in (42), the expression analogous to (40) is given by

$$\frac{d\bar{B}}{dt} = \frac{-K\bar{B}}{1 + Da(1 - \bar{B})\bar{h}} + O(Da^2), \tag{46}$$

as in Edwards et al. (1999).

Figure 5 is analogous to Fig. 3, as it shows the effect of varying μ_r on the ERC solution for the dissociation case. Again, the difference between the solution with μ_r infinite and μ_r finite is graphed. The magnitude of the deviations is similar to the association experiment, and the sign is negative, as in Fig. 4.

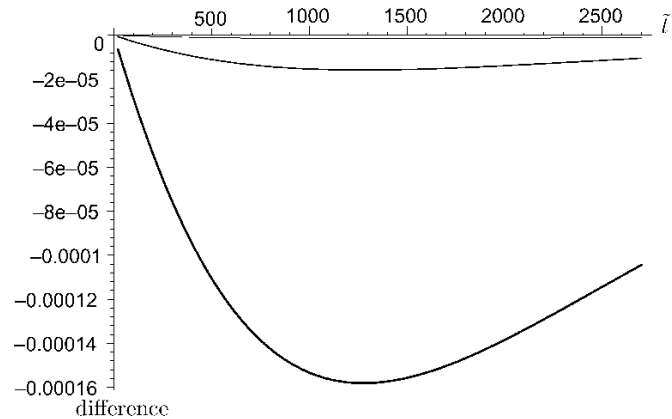

Fig. 5 Difference between ERC solution of (46) with $\mu_r = \infty$ (solid dextran) and μ_r finite for (in decreasing order of thickness) $\mu_r = 1, 10, 100$. Dissociation experiment.

6. Surface model, moderate *Da*

6.1. Association experiment

If $Da = O(1)$, (32) is nonlinear. Thus, to obtain analytic solutions we resort to small-time asymptotics by assuming a solution of the form

$$B(x,t) = B_\mathrm{i} + \beta(x)t + o(t), \quad t \to 0. \tag{47}$$

Substituting (47) into (32), we have, to leading order in t,

$$(1-B_\mathrm{i})\left(1 + Da\frac{v_0}{v_1}\beta\right) - \beta - KB_\mathrm{i} = \frac{Da(1-B_\mathrm{i})}{(3v_1)^{1/3}\Gamma(2/3)}\int_0^x \beta(x-\xi)\frac{\mathrm{d}\xi}{\xi^{2/3}},$$

which is a linear integral equation for the unknown $\beta(x)$. Taking the Laplace transform of the above and solving for the unknown $\hat{\beta}$, we obtain

$$\hat{\beta}(s) = \frac{\chi}{r_\mathrm{a}}\left(1 + \frac{v_\mathrm{a}^{1/3}}{s^{1/3}}\right)^{-1}, \tag{48}$$

$$r_\mathrm{a} = 1 - (1-B_\mathrm{i})Da\frac{v_0}{v_1}, \tag{49a}$$

$$v_\mathrm{a} = \frac{1}{3v_1}\left[\frac{Da(1-B_\mathrm{i})\Gamma(1/3)}{r_\mathrm{a}\Gamma(2/3)}\right]^3 = \frac{1}{3v_1}\left\{\frac{\Gamma(2/3)}{\Gamma(1/3)}\left[\frac{1}{Da(1-B_\mathrm{i})} - \frac{v_0}{v_1}\right]\right\}^{-3}, \tag{49b}$$

where the subscript "a" refers to "association experiment."

In (49b), we write the braced term in this fashion so the correction due to v_0 can be easily seen. Recall that in deriving (48), we have already taken an asymptotic limit for small v_0. Thus, we should expect that (48) will hold only for those Da where

$$\frac{1}{Da(1-B_\mathrm{i})} \gg \frac{v_0}{v_1}. \tag{50}$$

To calculate $\bar{B}$, we need the integral of β. By defining

$$\mathcal{I}[\beta;x] \equiv \int_0^x \beta(\xi)\,\mathrm{d}\xi, \tag{51}$$

we may write the average (31) in dimensional form, which we do with the aid of (14a):

$$\bar{B}(\tilde{t}) \sim B_\mathrm{i} + S\tilde{t}, \quad \tilde{t} \to 0, \qquad S = \frac{\tilde{k}_\mathrm{on}C_\mathrm{u}\{\mathcal{I}[\beta;x_\mathrm{max}] - \mathcal{I}[\beta;x_\mathrm{min}]\}}{x_\mathrm{max} - x_\mathrm{min}}. \tag{52}$$

Table 3 Parameter values for Figs. 6–9.

Parameter	Value
$\tilde{D}_f$ (cm^2 s^{-1})	2.8×10^{-7}
L (cm)	2.4×10^{-1}
R_T (mol cm^{-2})	10^{-12}

Inverting the transform in (48), we have

$$\mathcal{I}[\beta; x] = \frac{\chi e^{-\nu_a x}}{\nu_a r_a} \left[e^{\nu_a x} - 1 - |P(4/3, -\nu_a x)| + |P(5/3, -\nu_a x)| \right], \tag{53a}$$

where P is the normalized *lower* incomplete gamma function whose definition is

$$P(m/3, -\nu_a x) = \frac{\gamma(m/3, -\nu_a x)}{\Gamma(m/3)}. \tag{53b}$$

(The notation is from Abramowitz and Stegun (1972).)

To estimate the rate constants from experiments, we proceed as follows. Running an experiment to steady state will yield an estimate for α, and hence K, from (41). In order to calculate both the rate constants, we construct a linear fit to our small-time data, using the slope S in (52) to obtain $\tilde{k}_{on}$. The relationship between S and $\tilde{k}_{on}$ is not linear, as Da also depends on $\tilde{k}_{on}$. Using our estimates for K and $\tilde{k}_{on}$ together, we may calculate $\tilde{k}_{off}$.

In order to visualize the relationship between S and $\tilde{k}_{on}$, we construct a curve using the parameters in Table 3. For convenience, we define the new variable

$$k = 10^{-9} \tilde{k}_{on} \text{ mol s cm}^{-3}. \tag{54}$$

Substituting (54) and our parameters into (50), we find an upper bound on k where we can still use our solution:

$$k \ll 28 \mu_r. \tag{55}$$

In Fig. 6, we plot S versus $\log_{10} k$ for $\mu_r = \infty$ (the dextran case). This figure is exactly the same as Fig. 4 in Edwards (1999). Since we take $B_i = 0$ for the association case, $\chi = 1$ and our expression is independent of K. This will not be the case when we study a dissociation experiment in the next subsection.

We may asymptotically determine the behavior of S for small $\tilde{k}_{on}$, which corresponds to small k. For small k, $r_a \to 1$, so $\nu_a \to 0$ and we have

$$S \sim \tilde{k}_{on} C_u \chi, \qquad \tilde{k}_{on} \to 0. \tag{56}$$

Equation (56) merely shows that if there is no forward reaction ($\tilde{k}_{on} = 0$), then there will be no change in the bound concentration from the initial state ($S = 0$).

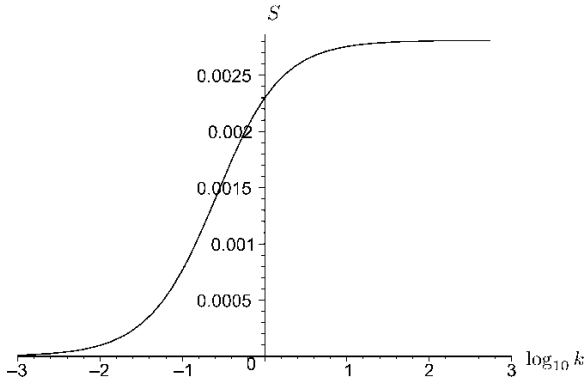

Fig. 6 S vs. $\log_{10} k$. Association experiment, $v_0 = 0$.

Unfortunately, we cannot ascertain the behavior in the case that $k \to \infty$ due to the form of (49b). As k increases, so will Da, eventually causing the bound in (50) to be violated. Essentially, because of the faster reaction, we cannot simply take the first-order convection correction; we must include additional terms in our analysis.

Next, we vary the viscosity ratio μ_r, as shown in Fig. 7. The functions plotted are the same as those in Figs. 2–5. In particular, we plot the difference between S in the solid dextran case with $\mu_r = \infty$ and the viscous-dextran case with μ_r finite. The corrections are again small, and they are positive, corresponding to increased transport with increased flow penetration. Also note that the graphs end for different values of k corresponding to the threshold in (55).

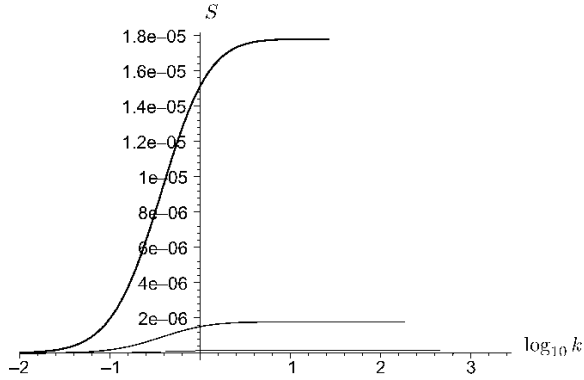

Fig. 7 Difference between S with $\mu_r = \infty$ (solid dextran) and μ_r finite vs. $\log_{10} k$ for (in decreasing order of thickness) $\mu_r = 1, 10, 100$. Association experiment.

6.2. *Dissociation experiment*

For the dissociation case, the initial condition is the steady state from the association problem, given in (41). Thus, the initial condition in (43a) holds even if we drop the subscript 0. In addition, the leading-order concentration is now 0, not 1. Thus, the derivation of the equation analogous to (48) becomes

$$\hat{\beta}(s) = -\frac{K}{\alpha r_{\mathrm{d}} s}\left(1 + \frac{v_{\mathrm{d}}^{1/3}}{s^{1/3}}\right), \tag{57}$$

$$r_{\mathrm{d}} = 1 - \left(\frac{K}{\alpha}\right) Da \frac{v_0}{v_1}, \tag{58a}$$

$$v_{\mathrm{d}} = \frac{1}{3v_1}\left[\frac{Da(K/\alpha)\Gamma(1/3)}{r_{\mathrm{d}}\Gamma(2/3)}\right]^3 = \frac{1}{3v_1}\left\{\frac{\Gamma(2/3)}{\Gamma(1/3)}\left[\frac{1}{Da(K/\alpha)} - \frac{v_0}{v_1}\right]\right\}^{-3}, \tag{58b}$$

where the subscript "d" refers to "dissociation experiment."

Examination of (57) shows that the sole structural change we have made is to replace χ by $-K/\alpha$ on the right-hand side; the other changes are limited to the parameters only. Thus, (53a) is replaced by

$$\mathcal{I}[\beta; x] = -\frac{K\mathrm{e}^{-v_{\mathrm{d}}x}}{v_{\mathrm{d}} r_{\mathrm{d}} \alpha}\left[\mathrm{e}^{v_{\mathrm{d}}x} - 1 - |P(4/3, -v_{\mathrm{d}}x)| + |P(5/3, -v_{\mathrm{d}}x)|\right]. \tag{59}$$

Using our new initial condition, we write our average as

$$\bar{B}(t) \sim \frac{1}{\alpha} + S\tilde{t}, \quad \tilde{t} \to 0,$$

where S is defined in (52). Note from (59) that the slope is now negative, as expected for our dissociation problem.

We carefully analyze the behavior of S with respect to k, beginning with the case where $v_0 = 0$. In Edwards et al. (1999), the authors kept K fixed and varied $\tilde{k}_{\mathrm{on}}$, which necessitated (tacitly) varying $\tilde{k}_{\mathrm{off}}$. In contrast, here we wish to keep $\tilde{k}_{\mathrm{off}}$ fixed, which means that K will vary as $\tilde{k}_{\mathrm{on}}$ does. We choose the value from Yarmush et al. (1996):

$$\tilde{k}_{\mathrm{off}} = \frac{8.9 \times 10^{-3}}{\mathrm{s}}, \tag{60}$$

which is in the middle of the range of $\tilde{k}_{\mathrm{off}}$ values in the experimental literature (see Edwards (1999) for more values).

Figure 8 shows a graph of S versus $\log_{10} k$. Careful readers will note that with the exception of the sign, which is just a change in convention, the main difference between the graphs here and in Edwards et al. (1999) is in the asymptotes, which we now examine.

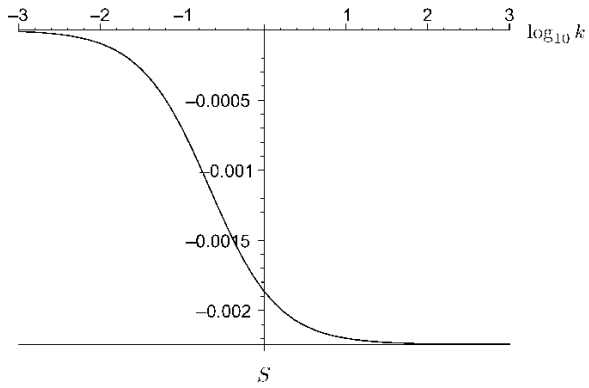

Fig. 8 *Thick line*: S vs. $\log_{10} k$, keeping $\tilde{k}_{\text{off}}$ fixed. *Thin line*: large-k asymptote. Dissociation experiment, $v_0 = 0$.

For the small-$\tilde{k}_{\text{on}}$ asymptote, we first note that

$$\lim_{\tilde{k}_{\text{on}}\to 0} \frac{K}{\alpha} = \lim_{K\to\infty} \frac{K}{K+1} = 1,$$

since with $\tilde{k}_{\text{off}}$ fixed, $\tilde{k}_{\text{on}} \to 0$ forces $K \to \infty$. Then to calculate the asymptote for S, we replace χ by $-K/\alpha$ in (56) to obtain

$$S \sim -\frac{\tilde{k}_{\text{on}} C_{\text{u}} K}{\alpha} = -\tilde{k}_{\text{on}} C_{\text{u}}, \qquad \tilde{k}_{\text{on}} \to 0, \tag{61}$$

where we have used (28a). Note that (61) holds for all v_0.

For the large-$\tilde{k}_{\text{on}}$ asymptote, we restrict ourselves to the case with no flow: $v_0 = 0$, $v_1 = 1$, which implies that $r_{\text{d}} = 1$. Upon noting that

$$\lim_{k_{\text{on}}\to\infty} \frac{\tilde{k}_{\text{on}} K}{\alpha} = \frac{\tilde{k}_{\text{off}}}{C_{\text{u}}}, \tag{62}$$

we may go on to calculate the limiting value of v_{d}:

$$\lim_{k_{\text{on}}\to\infty} v_{\text{d}} \equiv v_\infty = \frac{1}{3Pe_{\text{f}}} \left[\frac{\Gamma(1/3)}{\Gamma(2/3)} \frac{\tilde{R}_{\text{T}} H_{\text{f}}}{\tilde{D}_{\text{f}}} \frac{\tilde{k}_{\text{off}}}{C_{\text{u}}}\right]^3, \quad v_0 = 0. \tag{63}$$

This is the key difference from Edwards et al. (1999). In that work, K was kept fixed, so $v_{\text{d}} \to \infty$ as $\tilde{k}_{\text{on}} \to \infty$. This simplified $\mathcal{I}[\beta; x]$ greatly, leading to a relatively simple result for the asymptote. In our case, the asymptote is obtained by substituting v_∞ into (52) and (59). Note from (62) that when we multiply the $\tilde{k}_{\text{on}}$ from (52) with the K/α from (59), we will get a finite result. With the parameters chosen one can verify that the correct asymptote is

$$S = -2.24 \times 10^{-3},$$

as shown in Fig. 8.

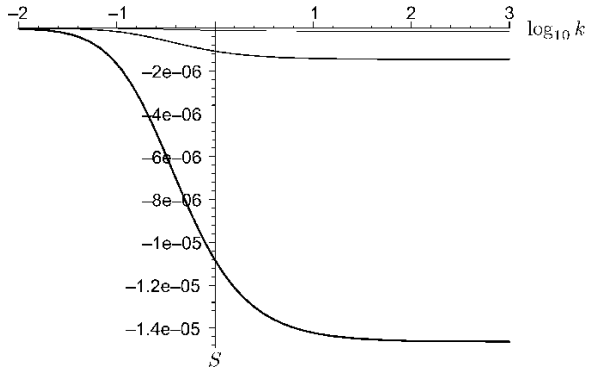

Fig. 9 Difference between S with $\mu_r = \infty$ (solid dextran) and μ_r finite vs. $\log_{10} k$ for (in decreasing order of thickness) $\mu_r = 1, 10, 100$. Dissociation experiment.

Next we vary the viscosity ratio μ_r. From (58b) we see that the relevant inequality replacing (50) is

$$\frac{\alpha}{Da\, K} \gg \frac{v_0}{v_1}.$$

Substituting our parameters into the above, we have

$$2.21 \ll 69.4\mu_r,$$

where we have used (60) and (62). Note that this is no longer a bound on k; it is simply a bound on μ_r, which is always satisfied experimentally. Thus, our expressions do not break down for large k as in the association case.

Figure 9 is analogous to Fig. 7 for the dissociation case, showing the difference found when assuming that the dextran is viscous, rather than solid. Note that the change to S is negative (enhancing dissociation), but quite small. Note also that the curves extend all the way to the right; they are not truncated by a bound on k.

7. Conclusions

To understand certain biological systems, scientists need accurate estimates for the rate constants of the underlying chemical reactions. With the advent of SPR technology and the BIAcore, scientists have access to real-time data of binding in a controlled setting. However, such technological advances are useless without the necessary mathematical models to interpret the data properly.

In order to help explain anomalous readings from the BIAcore, it has been theorized (Witz, 1999) that buffer flow from the channel penetrates into the dextran gel layer. This would introduce convection effects into the layer, whereas previous models considered only diffusive effects. Since convection is a more efficient

mode of transport in the BIAcore, it was suggested that such flow penetration would speed the reaction.

Though our results confirm this hypothesis, they also demonstrate that, at least in the case of a surface reaction model, these penetration effects are negligible. Though we developed our theory by treating the dextran gel as a viscous fluid, the thinness of the gel layer indicates that even more realistic models, such as the polymer brush model in Witz (1999), will not produce appreciable changes in the results obtained.

The small parameter H_r manifests itself in the small size of the velocity within the dextran gel. The correction for small H_r is most succinctly stated in (32); namely, the slip condition at the flow–gel interface introduces a local depletion term that complements the integral depletion term from the no-penetration case.

Since (32) is a nonlinear equation, we obtained analytical results in two ways. Since most experiments are designed to have $Da \ll 1$ to mimic the standard well-mixed kinetic theory, we calculated the first-order correction in the case that $Da \to 0$. We showed that the only difference between the penetration and no-penetration case is the form of the function $h(x)$, as defined in (38). Because of this similarity, we could derive not only solution profiles for B, but also an ERC equation, which can be used to fit sensogram data directly. However, as discussed earlier, none of the corrections due to penetration were appreciable.

In order to analyze experiments that cannot be designed such that $Da \ll 1$, we also presented the theory for the moderate Da case. Here we may fit a short-time slope of the sensogram data in order to construct estimates of the rate constants. The corrections due to flow penetration manifested themselves only in the parameter definitions in (49); the rest of the theory is the same as in the no-penetration case. Because of the nature of these corrections, we could not construct results for cases where $Da \to \infty$; however, these cases do not occur experimentally.

For completeness, we examined both association and dissociation experiments, providing (when possible) both large- and small-$\tilde{k}_{on}$ behavior of the small-time solution. For the dissociation experiments, we kept $\tilde{k}_{off}$ fixed, in contrast to Edwards et al. (1999). However, any differences between the results of this paper and that one were minor, not fundamental. In any event, the corrections from the no-penetration case were small.

It can be shown that the same negligible corrections will also occur when the reaction zone is considered to be a layer, not a surface (Edwards, submitted). Thus, flow penetration effects are not a likely candidate for explaining anomalous BIAcore measurements, and other avenues, such as steric hindrance effects or conformational changes, should be explored.

Acknowledgements

This work was supported by NIGMS grant 1R01GM067244-01. Portions of this manuscript were prepared during sabbatical stays at the Mathematical Biosciences Institute at the Ohio State University and the University of Maryland, Baltimore County.

Table A.1 Additional parameter values of interest.

Parameter	Value	Reference
H_f (cm)	5×10^{-3}	BIAcore, Inc. (undated)
H_g (cm, CM5 chip)	10^{-5}	Hoffman et al. (2000)
H_g (cm, F1 chip)	3×10^{-6}	Maquart (2005); Parsons and Stockley (1997)
V (cm s^{-1}, upper bound)	40	Myszka (1997)
ν (cm^2 s^{-1})	10^{-2}	Bird et al. (1960)

Appendix

Table A.1 lists additional parameters needed for our computations. First, we verify that the laminar flow assumption is indeed valid. The appropriate Reynolds number for the flow is

$$Re = \frac{V_f H_f}{\nu},$$

where ν is the kinematic viscosity of the buffer fluid, which we take to be that of water. Using the parameters in Table A.1 in the equation above, we obtain $Re = 20$ as an upper bound (since the value for V_f in Table A.1 is an upper bound). Thus, we are well within the laminar regime.

BIAcore sensor chips come in three thicknesses. Chips such as the C1 have no dextran layer at all (Hoffman et al., 2000), thus eliminating flow penetration from the analysis. Unfortunately, only certain types of receptors can be bound directly to the gold surface. The thicknesses of the other types of chips are given in Table A.1. We note from these values that the upper bound on H_r is given by

$$H_r = \frac{H_g}{H_f} = 2 \times 10^{-3},$$

and with the F1 chip it is even smaller.

From Table 2 we have that $Pe_f^{-1/3} = 1.39 \times 10^{-1}$. Thus, as indicated in the text, the gel layer is much thinner than the unstirred layer. In particular, this implies that

$$v_0 = Pe_f^{1/3} v_f(0) = \frac{1.44 \times 10^{-2}}{2 \times 10^{-3} + \mu_r}.$$

Since $\mu_r \geq 1$ by definition, the flow in the gel layer is going to be very small. Because $v_1 \approx 1$, the actual numerical correction to our solutions will also be very small, since

$$\frac{v_0}{v_1} = \frac{1.44 \times 10^{-2}}{\mu_r - 4 \times 10^{-6}}.$$

References

Abramowitz, M., Stegun, I.A. (Eds.), 1972. Handbook of Mathematical Functions, Applied Mathematics Series, vol. 155. US Department of Commerce, Washington.

BIAcore, Inc., undated. System Manual Version 1.1. BIAcore, Inc., Uppsala.

Bird, R.B., Stewart, W.E., Lightfoot, E.N., 1960. Transport Phenomena. Wiley, New York.

Boireau, W., Zeeh, J.C., Puig, P.E., Pompon, D., 2005. Unique supramolecular assembly of a redox protein with nucleic acids onto hybrid bilayer: Towards a dynamic DNA chip. Biosens. Bioelectron. 20, 1631–1637.

Davis, S.J., Davies, E.A., Barclay, A.N., Daenke, S., Bodian, D.L., Jones, E.Y., Stuart, D.I., Butters, T.D., Dwek, R.A., Van der Merwe, P.A., 1995. Ligand binding by the immunoglobulin superfamily recognition molecule CD2 is glycosylation-independent. J. Biol. Chem. 270, 369–375.

Edwards, D.A., 1999. Estimating rate constants in a convection-diffusion system with a boundary reaction. IMA J. Appl. Math. 63, 89–112.

Edwards, D.A., 2000. Biochemical reactions on helical structures. SIAM J. Appl. Math. 60, 1425–1446.

Edwards, D.A., 2001. The effect of a receptor layer on the measurement of rate constants. Bull. Math. Biol. 63, 301–327.

Edwards, D.A., 2004. Refining the measurement of rate constants in the BIAcore. J. Math. Biol. 49, 272–292.

Edwards, D.A., submitted. Convection effects in thin reaction zones: Applications to BIAcore. SIAM J. Appl. Math.

Edwards, D.A., Goldstein, B., Cohen, D.S., 1999. Transport effects on surface-volume biological reactions. J. Math. Biol. 39, 533–561.

Edwards, D.A., Jackson, S.A., 2002. Testing the validity of the effective rate constant approximation for surface reaction with transport. Appl. Math. Lett. 15, 547–552.

Edwards, D.A., Swaminathan, S., 2005. The effect of receptor site nonuniformity on the measurement of rate constants. Appl. Math. Lett. 18, 1101–1107.

Hoffman, T.L., Canziani, G., Jia, L., Rucker, J., Doms, R.W., 2000. A biosensor assay for studying ligand-membrane receptor interactions: Binding of antibodies and HIV-1 env to chemokine receptors. Proc. NAS 97, 11215–11220.

Joss, L., Morton, T.A., Doyle, M.L., Myszka, D.G., 1998. Interpreting kinetic rate constants from optical biosensor data recorded on a decaying surface. Anal. Biochem. 261, 203–210.

Karlsson, R., Fält, A., 1997. Experimental design for kinetic analysis of protein–protein interactions with surface plasmon resonance biosensors. J. Immunol. Methods 200, 121–133.

Karlsson, R., Michaelson, A., Mattson, L., 1991. Kinetic analysis of monoclonal antibody–antigen interactions with a new biosensor based analytical system. J. Immunol. Methods 145, 229–240.

Karlsson, R., Roos, H., Fägerstam, L., Persson, B., 1994. Kinetic and concentration analysis using BIA technology. Methods 6, 99–110.

Liedberg, B., Lundstrom, I., Stenberg, E., 1993. Principles of biosensing with an extended coupling matrix and surface-plasmon resonance. Sens. Actuators B 11, 63–72.

Maquart, A., 2005. SPR pages: Sensor chips overview. Online: http://home.hccnet.nl/ja.marquart/Sensorchips/Sensorchips.htm.

Mason, T., Pineda, A.R., Wofsy, C., Goldstein, B., (1999). Effective rate models for the analysis of transport-dependent biosensor data. Math. Biosci. 159, 123–144.

Minunnia, M., Tombellia, S., Mascinia, M., Biliab, A., Bergonzib, M.C., Vincieribi, F., 2005. An optical DNA-based biosensor for the analysis of bioactive constituents with application in drug and herbal drug screening. Talanta 65, 578–585.

Myszka, D.G., 1997. Kinetic analysis of macromolecular interactions using surface plasmon resonance biosensors. Curr. Opin. Biotechnol. 8, 50–57.

Myszka, D.G., He, X., Dembo, M., Morton, T.A., Goldstein, B., 1998. Extending the range of rate constants available from BIAcore: Interpreting mass transport influenced binding data. Biophys. J. 75, 583–594.

O'Shannessy, D.J., Brigham-Burke, M., Peck, K., 1992. Immobilization chemistries suitable for use in the BIAcore surface plasmon resonance detector. Anal. Biochem. 205, 132–136.

Parsons, I.D., Stockley, P.G., 1997. Quantitation of the *Escherichia coli* methionine repressor–operator interaction by surface plasmon resonance is not affected by the presence of a dextran matrix. Anal. Biochem. 254, 82–87.

Phillies, G.D.J., 1985. Diffusion of bovine serum-albumin in a neutral polymer-solution. Biopolymers 24, 379–386.

Qian, S., 2004. Personal communication.

Samsonova, J.V., Uskova, N.A., Andresyuk, A.N., Franek, M., Elliott, C.T., 2004. Biacore biosensor immunoassay for 4-nonylphenols: Assay optimization and applicability for shellfish analysis. Chemosphere 57, 975–985.

Schuck, P., 1996. Kinetics of ligand binding to receptor immobilized in a polymer matrix, as detected with an evanescent wave biosensor. I. A computer simulation of the influence of mass transport. Biophys. J. 70, 1230–1249.

Sikavitsas, V., Nitsche, J.M., Mountziaris, T.J., 2002. Transport and kinetic processes underlying biomolecular interactions in the BIACORE optical biosensor. Biotechnol. Prog. 18, 885–897.

Szabo, A., Stolz, L., Granzow, R., 1995. Surface plasmon resonance and its use in bio-molecular interaction analysis (BIA). Curr. Opin. Struct. Biol. 5, 699–705.

Varadarajan, R., Sharma, D., Chakraborty, K., Patel, M., Citron, M., Sinha, P., Yadav, R., Rashid, U., Kennedy, S., Eckert, D., Geleziunas, R., Bramhill, D., Schleif, W., Liang, X., Shiver, J., 2005. Characterization of gp120 and its single-chain derivatives, gp120-$CD4_{D12}$ and gp120-M9: Implications for targeting the $CD4_i$ epitope in human immunodeficiency virus vaccine design. J. Virol. 79, 1713–1723.

Ward, L.D., Winzor, D.J., 2000. Relative merits of optical biosensors based on flow-cell and cuvette designs. Anal. Biochem. 285, 179–193.

Witz, J., 1999. Kinetic analysis of analyte binding by optical biosensors: Hydrodynamic penetration of the analyte flow into the polymer matrix reduces the influence of mass transport. Anal. Biochem. 270, 201–206.

Wofsy, C., Goldstein, B., 2002. Effective rate models for receptors distributed in a layer above a surface: Application to cells and BIAcore. Biophys. J. 82, 1743–1755.

Yarmush, M.L., Patankar, D.B., Yarmush, D.M., 1996. An analysis of transport resistance in the operation of BIAcore^{TM}; implications for kinetic studies of biospecific interactions. Mol. Immunol. 33, 1203–1214.

Zheng, Y., Rundell, A., 2003. Biosensor immunosurface engineering inspired by B-cell membrane-bound antibodies: Modeling and analysis of multivalent antigen capture by immobilized antibodies. IEEE Trans. Nanobiol. 2, 14–25.